PWM TECHNIQUE WITH VARIABLE CARRIER WAVE FREQUENCY TO REDUCE SWITCHING LOSS IN GRID-CONNECTED PV INVERTER

KỸ THUẬT ĐIỀU RỘNG XUNG TRONG NGHỊCH LƯU NỐI LƯỚI ĐỂ GIẢM TỔN HAO CHUYỂN MẠCH

Tran Quang Tho[1], Truong Viet Anh[1], Le Minh Phuong[2]
[1] Ho Chi Minh City University of Technology and Education
[2] Ho Chi Minh City University of Technology

TÓM TẮT

Nguồn điện phân tán là một trong những nguyên nhân ảnh hưởng đến chất lượng điện năng. Việc sử dụng ngày càng nhiều các nguồn điện phân tán trong hệ thống điện đòi hỏi tiêu chuẩn nối lưới ngày càng nghiêm ngặt. Để giảm sóng hài dòng điện trong các bộ nghịch lưu nối lưới nhằm thỏa mãn tiêu chuẩn nối lưới thường sử dụng phương pháp tăng tần số chuyển mạch nhưng cũng làm tăng tổn hao chuyển mạch trong bộ nghịch lưu. Bài báo này đề nghị một kỹ thuật điều chế độ rộng xung với tần số chuyển mạch thay đổi trong nửa chu kỳ lưới để giảm tổn hao chuyển mạch của nghịch lưu. Kết quả mô phỏng của một hệ thống nghịch lưu nối lưới trên Matlab/Simulink cho thấy rằng tổn hao chuyển mạch của kỹ thuật đề nghị thấp hơn trường hợp tần số chuyển mạch cố định.

Từ khóa: *Điều chế độ rộng xung (PWM), độ méo dạng hài toàn phần (THD), nguồn điện phân tán (DG).*

ABSTRACT

The increasing application of distributed power generations into the power system leads to a grid interconnection requirements of THD stricter and stricter. The reduction of current THD of grid-connected inverters to satisfy the grid code by increasing of switching frequency in PWM of inverters is one of popular methods but increases switching loss. The aim of this paper is to propose a PWM technique with variable switching frequency to reduce switching loss in inverters. The simulation results of a grid-connected inverter system in Matlab/Simulink show that the switching loss of the proposed technique is lower than the constant switching frequency.

Keywords: *pulse width modulation (PWM), total harmonic distortion (THD), distributed generation (DG)*

I. INTRODUCTION

The increasing application of distributed generations into power system such as wind, solar energies, and fuel cells thanks to strong development of grid-connected inverter systems [1] for sustainability and environment with enormous potentials [2]. However, the grid-connected inverters inject significantly current harmonics into power network and effect adversely on power quality of system. So, the harmonic attenuation is expected to be significantly more stringent in order to meet IEEE standard 929-2000 [3], 1547-2009 [4], [5].

The inverters with sine pulse width modulation (SPWM) are used very popular in renewable energy converters [6]-[9]. The increase of inductance in filters is one of popular methods to reduce output current harmonics of grid-connected inverters. But it also has disadvantages of costs, dimensions of devices. The higher switching carrier frequency to reduce current harmonic content of inverters results in the higher switching

loss and overheating in components [10].

The technique in [11] used the H∞ controller instead of conventional PI controller in conditions of grid impedance variations with enough high frequency attenuation to keep the control loop stable. However, the determination of weighting function has complex and calculation burden. It also requires time and parameters of grid to track the weighting functions.

The variable switching frequency technique proposed in [12] to reduce switching loss in inverters also requires the accurate model of ripple current and the complicated calculations cause robustness and dynamic response low. In addition, the usages of fixed load and very high switching frequency are not suitable for real grid-connected inverters. Moreover, very low switching frequency of current at the vicinity of zero is a big obstacle to digital electronic meters and electric motors.

A different technique with variable switching frequency in [13] based on the estimated model of TDD. However, the requirements of parameters of filter, time of computation to select the optimal switching frequency and level variation of switching frequency make the strategy with poor dynamic response and robustness performance.

The multi-level inverters are also used [14] to reduce current harmonic content. But they also have complicated control and many power switches. To reduce switching loss and current THD, the hysteresis technique in [15] exposed the dependence of measured current error, current sensor. So, it is also not robust.

This paper proposes the technique of SPWM with variable switching frequency to reduce switching loss in grid-connected inverters. The aim of paper is to determine the optimal switching frequency of inverter in every fundamental period to reduce switching loss with subject to constant current THD.

II. ANALYSIS OF CURRENT RIPPLE

The relationship between current THD and switching loss in inverter is very close. The selection of optimal switching frequency to reduce current THD of inverters is complicated problem and has a very important meaning.

An H-bridge grid-connected single phase inverter with unipolar PWM as shown in Figure.1 is used to analyze in this paper. The power factor is always kept as unit because of injecting active power into grid source.

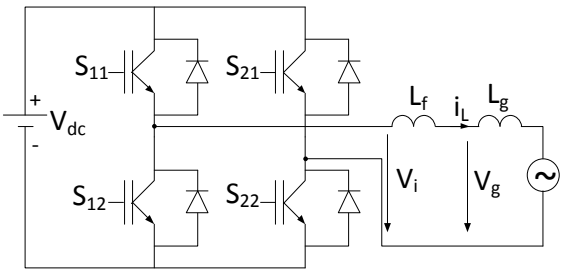

Figure 1. H-bridge grid-connected inverter.

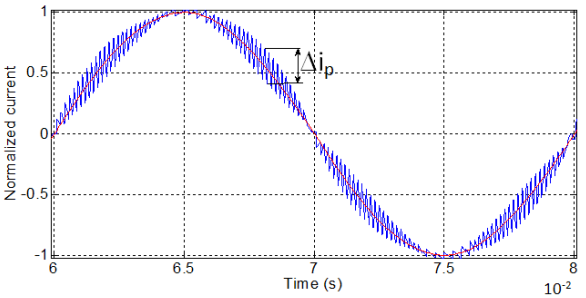

Figure 2. Output current waveform of unipolar H-bridge single phase inverter.

It is assumed that the switching frequency of inverter is much higher than the frequency of control signal, effect of dead time is negligible and the inductance of filter is fixed.

The loss of IGBTs and diodes consists of switching loss, conduction loss, and other losses. It is also assumed that the conduction loss is not dependent on switching frequency of inverter and the switching loss is linearly dependent on the switched current and switching frequency for one switching cycle.

The output current waveform of unipolar H-bridge single phase inverter is shown in Figure.2.

Based on the superposition principle, the inverter output current consists of the fundamental current and the ripple current.

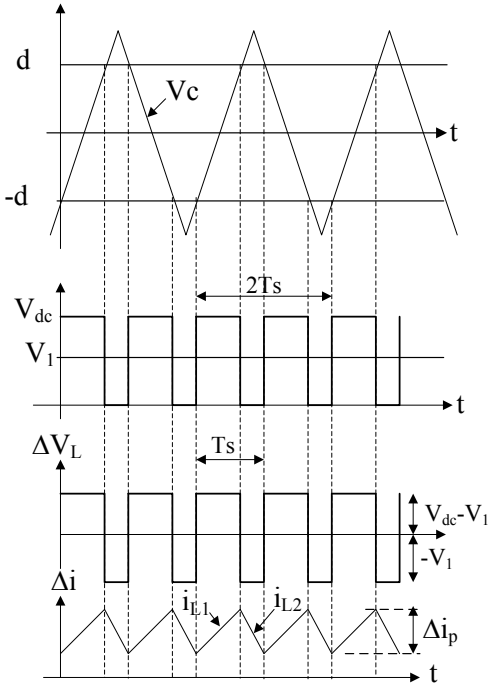

Figure 3. Current waveforms.

The wave forms in Figure.3 show that inverter output current increases and decreases in every half of the switching cycle of carrier wave. In the positive half cycle of carrier cycle, duty cycle d(t), the increase of peak-to-peak current ripple i_{L1} can be calculated as (1):

$$i_{L1} = \frac{V_{dc} - V_{dc}.d(t)}{L_f} d(t).T_s \qquad (1)$$

Where L_f is inductance of output filter of inverter, V_{dc} is the DC input voltage value of inverter and Ts is the half of carrier wave period. Equation (1) can also be rewritten as:

$$i_{L1} = \frac{V_{dc}T_s}{L_f}\left(1 - d(t)\right)d(t) \qquad (2)$$

The similar calculation for the decrease of current ripple i_{L2} is (3) and (4).

$$i_{L2} = \left| \frac{-V_{dc} + V_{dc}.(-d(t))}{L_f}(-d(t).T_s) \right| \qquad (3)$$

Equation (3) can be rewritten as:

$$i_{L2} = \frac{V_{dc}T_s}{L_f}\left|1 + d(t)\right|(-d(t)) \qquad (4)$$

Adding (2) and (4) for both the positive and negative half cycles of d(t) yields (5):

$$\Delta i_L = \frac{V_{dc}T_s}{L_f}\left|1 - d(t)\right|\left|d(t)\right| \qquad (5)$$

The control signal d(t) is expressed as:

$$d(t) = m.\sin(\omega t) \qquad (6)$$

Where m is the modulation index of amplitude and ω is the velocity frequency of grid source. Replacing (6) into (5), yields the peak-peak current ripple (7) as:

$$\Delta i_p = \frac{V_{dc}T_s}{L_f}\left(1 - m.\left|\sin(\omega t)\right|\right).m.\left|\sin(\omega t)\right| \qquad (7)$$

The root mean square value of every half of switching cycle equals the peak value divided by $\sqrt{3}$ as:

$$\Delta I_p = \frac{V_{dc}T_s}{L_f 2\sqrt{3}}\left(1 - m.\left|\sin(\omega t)\right|\right).m.\left|\sin(\omega t)\right| \qquad (8)$$

The normalized equation for the peak-peak current ripple is

$$\Delta I_p{}^* = \left(1 - m.\left|\sin(\omega t)\right|\right).m.\left|\sin(\omega t)\right| \qquad (9)$$

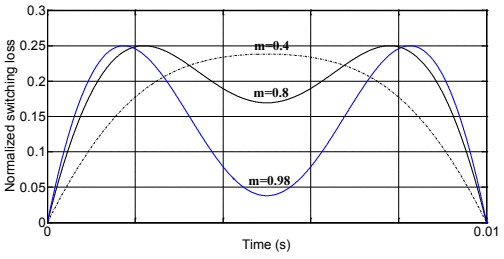

Figure 4. The normalized peak-peak current ripple with different values of m in every half of fundamental period.

The equation (9) shows the time variation of normalized peak-peak current ripple with different values of modulation index m in condition of constant carrier frequency as Figure 4.

As assumed above, the switching loss in every switching cycle is linearly dependent on the switched fundamental current and the switching frequency. It is also assumed that

the effect of current ripple on switching loss is neglected. The switching loss is expressed as:

$$\Delta P_{sw} = C_1.|i_1(\omega t)|.f_{sw}(\omega t) \qquad (10)$$

Where the constant C_1 depends on the DC voltage V_{dc} and the inductance of filter L_f, and $i_1(\omega t)$ is value of the fundamental instantaneous current flowing in the power device. The equation (10) can be rewritten as:

$$\Delta P_{sw} = C_1.|i_1(\omega t)|.\frac{1}{T_s(\omega t)} \qquad (11)$$

Where $T_s(\omega t)$ is the switching function

The average switching loss in one half of fundamental period is

$$\Delta P_{sw} = C_1.\sqrt{2}.I_1.\frac{1}{\pi}\int_0^{\pi}\frac{|\sin(\omega t)|}{Ts(\omega t)}d(\omega t) \qquad (12)$$

1. The constant frequency carrier wave

When the frequency of carrier wave is constant, the switching cycle Ts(ωt) is calculated by using (8) as

$$Ts(\omega t) = \frac{\Delta I_p.2\sqrt{3}.L_f}{V_{dc}.|1-m.\sin(\omega t)|.m.|\sin(\omega t)|} \qquad (13)$$

The RMS value of current ripple in the half of fundamental period is

$$\Delta I = \sqrt{\frac{1}{\pi}\int_0^{\pi}\Delta I_p^2 d(\omega t)} = \sqrt{\frac{1}{\pi}\int_0^{\pi}\left[\frac{V_{dc}Ts}{L_f 2\sqrt{3}}(1-m.|\sin(\omega t)|).m.|\sin(\omega t)|\right]^2 d(\omega t)} \qquad (14)$$

The current THD has the following relation to RMS current ripple as:

$$THD = \frac{\Delta I}{I_1} \qquad (15)$$

Where I_1 is the RMS value of fundamental current of the inverter.

Substituting (13) into (12) yields the switching loss as:

$$\Delta P_{sw} = \frac{C_1.\sqrt{2}.I_1}{2\sqrt{3}.L_f}.\frac{V_{dc}}{\pi} x\int_0^{\pi}\frac{|1-m.\sin(\omega t)|.m.|\sin(\omega t)|^2}{\Delta I_p}d(\omega t) \qquad (16)$$

2. The proposed variable frequency carrier wave

The active power is normally injected into the utility by the grid-connected PV inverter. So, the voltage and current of inverter output are always in phase. In addition, the phase angle is also ignored in this paper by the technique of current control.

The Figure 4 shows that the normalized peak-peak current ripple varies in the half of fundamental period with constant frequency carrier wave. So, the current ripple of inverter can be reduced by varying appropriately frequency of carrier wave in half of fundamental period. The frequency of carrier wave needs to increase in areas of high current ripple to reduce current THD and to decrease in areas of low current ripple to reduce switching loss.

Based on equations (14) and (15), they show that it is possible to reduce current THD by varying appropriately frequency of carrier wave f_{sw}. So, the optimal frequency of carrier wave is based on equation (8) and keep switching loss ΔP_{SW} minimum according to (12) and under the constraint that ΔI is constant according to (14).

The equation (8) shows that the current ripple is a variable quantity in every half of fundamental period. To ensure current THD (%) constant, the current ripple is also relative constant to fundamental current. It means that

$$\Delta I_p(\%) = \frac{\Delta I_p}{i_1(\omega t)}(100\%) = \frac{\Delta I_p}{I_1\sqrt{2}\sin(\omega t)}(100\%) \qquad (17)$$

Substituting (8) into (17) yields:

$$\Delta I_p(\%) = \frac{V_{dc} Ts}{L_f 2\sqrt{3}} \cdot \frac{\left(1 - m.\left|\sin(\omega t)\right|\right).m.\left|\sin(\omega t)\right|}{I_1 \sqrt{2}\sin(\omega t)}(100\%) \quad (18)$$

The switching cycle is inferred as

$$T_s(\omega t) = \frac{\Delta I_p(\%) L_f 2\sqrt{6} I_1}{(100\%) V_{dc}} \cdot \frac{\left|\sin(\omega t)\right|}{\left(1 - m.\left|\sin(\omega t)\right|\right).m.\left|\sin(\omega t)\right|} \quad (19)$$

The switching cycle is also rewritten as:

$$T_s(\omega t) = C_2 \Delta I_p(\%) \frac{\left|\sin(\omega t)\right|}{\left(1 - m.\left|\sin(\omega t)\right|\right).m.\left|\sin(\omega t)\right|} \quad (20)$$

Where the constant C_2 depends on L_f and V_{dc}, and RMS value of fundamental current I_1. So, the switching cycle must vary as (20) with a given constant current THD (%). The normalized switching frequency is calculated as (21) from equation (20) and shown as Figure 5.

$$f_{sw}^*(\omega t) = \frac{\left(1 - m.\left|\sin(\omega t)\right|\right).m.\left|\sin(\omega t)\right|}{\left|\sin(\omega t)\right|} \quad (21)$$

The normalized switching loss is determined as

$$\Delta P_{sw}^* = \left|\sin(\omega_1 t)\right|.f_{sw}^*(\omega t) = \left(1 - m.\left|\sin(\omega t)\right|\right).m.\left|\sin(\omega t)\right| \quad (22)$$

However, the switching frequency could not exceed the limit of maximum switching frequency of power IGBTs and need to be limited as (23) and Figure 6.

$$f_{sw}(\omega t) \le f_{\max} \quad (23)$$

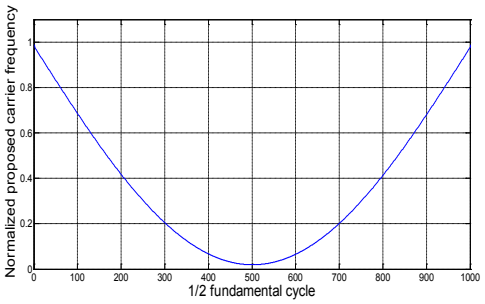

Figure 5. The normalized switching frequency in half of fundamental period.

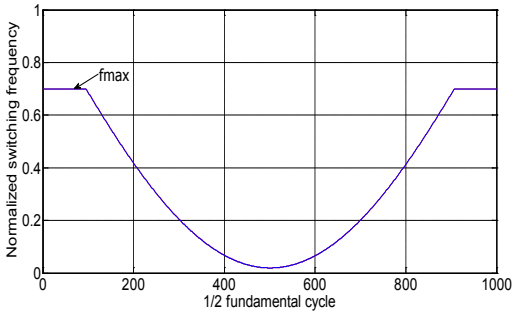

Figure 6. The normalized switching frequency with limit of f_{max} in half of fundamental period.

III. SYSTEM DESCRIPTION

The proposed control scheme of single phase grid-connected system that has been simulated in Matlab/Simulink and shown as Figure 7 includes power circuit of H-bridge inverter with unipolar PWM technique and the reference signal is based on current controller. The phase angle ωt of grid voltage V_g is determined by phase lock loop PLL.

$$I_{ref} = I_{ref\_\max} \sin(\omega t + dec) \quad (24)$$

Where dec regulated by PI controller of reactive power Q_{ref}. The current I_g injected into grid source is regulated by current controller PI as (25).

$$V_{ref} = \left(I_{ref} - I_g\right)\left(K_{p\_I} + \frac{1}{s}K_{i\_I}\right) \quad (25)$$

The parameters of PI controllers are determined by PSO method.

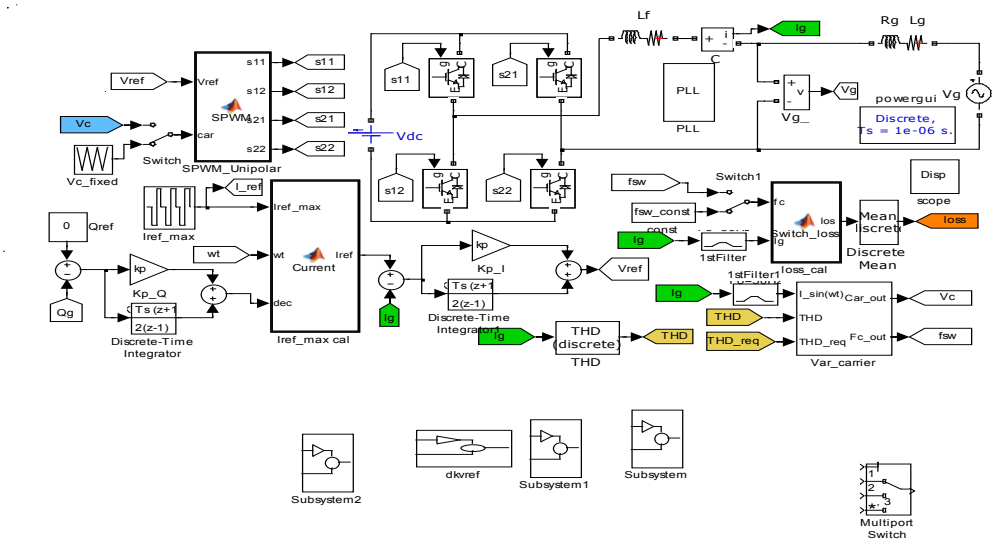

Figure 7. The simulated inverter system in Matlab/Simulink.

The carrier wave signal is calculated by block Var_carrier with inputs of measured grid current I_g, THD and required current THD. The switching loss of simulated cases is calculated by block loss_cal and the simulated results are displayed in block scope. Table 1 is the summary of the system parameter values.

Table 1. The system parameters

Parameter	Description	Value
L_g	Grid inductance	0.1mH
R_g	Resistance of L_g	0.01W
L_i	Inverter inductance	2.2mH
R_i	Resistance of L_i	0.01W
Vdc	DC voltage value	320V
Vg	Grid voltage	220VAC
f	Fundamental frequency of grid	50Hz

IV. SIMULATED RESULTS AND DISCUSSION

The simulated results of the two switching frequency cases will be compared in this section for the performances of I_{ref_max} =5A and 15A. The required current THD is always held lower than 5% for all cases. The parameters of table 1 are the same for both cases.

1. Simulated results with I_{ref_max} =5A

The simulated results for the first performance with the reference current I_{ref_max}=5A are shown in figures from Figure 8a to Figure 8c.

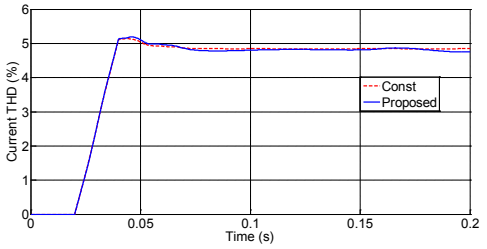

Figure 8a. Grid current THD with I_{ref_max}=5A

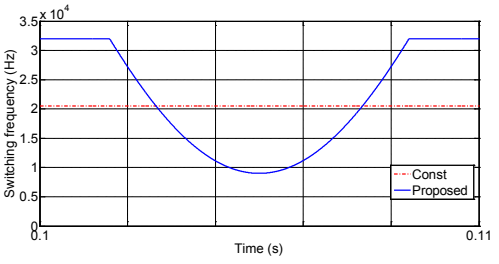

Figure 8b. Switching frequency in half of fundamental period with I_{ref_max}=5A

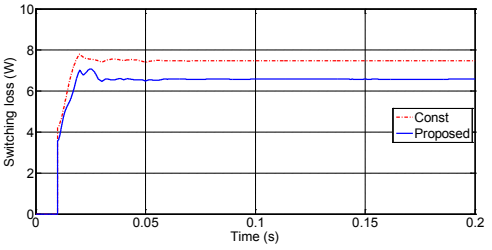

Figure 8c. Switching loss with Iref_max=5A.

The current THD is the same for both cases of constant switching frequency and proposed variable switching frequency as Figure 8a.
The switching frequency in half of fundamental period of the proposed technique is also shown in Figure 8b and the constant switching frequency is 20.5 kHz. The switching losses in Figure 8c are 7.48W for the constant frequency case and 6.57W for the proposed one. It means that the switching loss of proposed technique saves 12.16%.

2. Simulated results with I_{ref_max} =15A

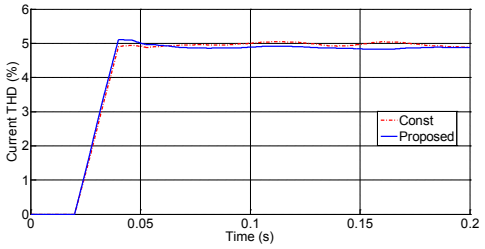

Figure 9a. Current THD with Iref_max=15A.

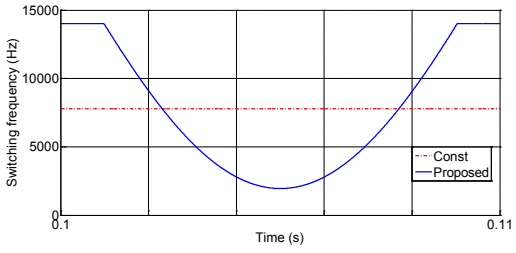

Figure 9b. Switching frequency in half of fundamental period with Iref_max=15A.

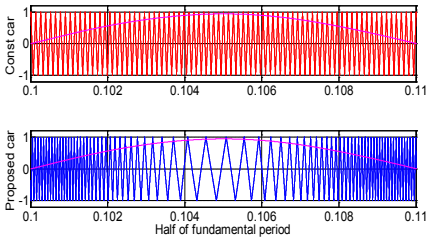

Figure 9c. Carrier wave variation in the half of fundamental period.

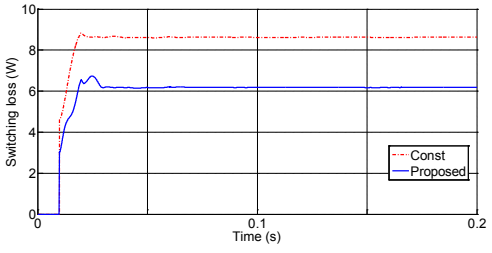

Figure 9d. Switching loss with Iref_max=15A.

The simulated results of with the reference current I_{ref_max}=15A are also shown in figures from Figure 9a to Figure 9f.

The current THD is also held lower than 5% for both cases as Figure 9a. The switching frequency in half of fundamental period is also shown in Figure 9b and Figure 9c. The constant switching frequency of this performance is 7.8 kHz.

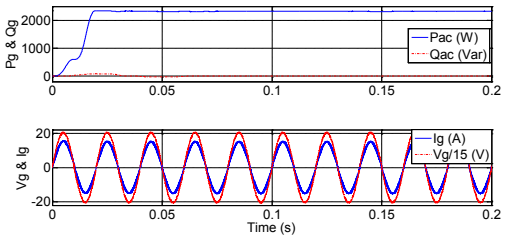

Figure 9e. Pg, Qg, Ig and Vg.

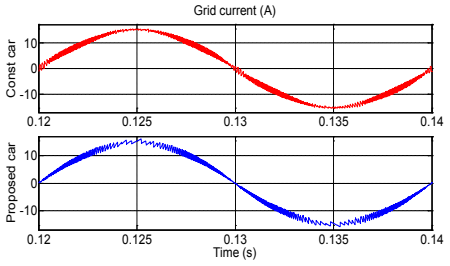

Figure 9f. Grid current.

The switching losses in Figure 9d are 8.664W for the constant frequency case and 6.179W for the proposed one. It also means that the switching loss of proposed strategy saves up to 28.68%. In addition, the quantities in Figure 9e also show that responses of active power Pg, reactive power Qg injected into the grid source, synchronization of grid current Ig and voltage Vg are very good (<0.06s).

Moreover, the grid currents for both cases in Figure 9f also show that current ripple at the vicinity of zero of the proposed technique is better than the constant one.

V. CONCLUSION

It is very difficult to select the switching frequency in the grid-connected inverters by balance between reducing switching loss and current THD. The proposed technique of variable switching frequency in half of fundamental period of this paper showed that

switching loss reduces significantly compared with the constant switching frequency with the same given current THD. In addition, the usage of current signal to control in this technique allows regardless of phase angle between voltage and current. The analysis of simulated results also showed that the current ripple at the vicinity of zero of the proposed technique is better than the constant one. The higher power application results in the higher switching loss saving. The current THD can also reduce significantly with the same given switching loss in this technique.

REFERENCES

[1] F. Blaabjerg, Z. Chen, and S.B. Kjaer, Power electronics as efficient interface in dispersed power generation systems, *IEEE Trans. on Power Electronics*, Vol.19, No. 5, p. 1184-1194, September 2004.

[2] E. Liu and J. Bebic, Distribution system voltage performance analysis for high-penetration photovoltaics, *GE Global Res., Niskayuna, NY, Rep. NREL/SR*-581-42298, 2008

[3] IEEE Recommended Practice for Utility Interface of Photovoltaic (PV) Systems, *IEEE Standard* 929, 2000.

[4] IEEE Application Guide for IEEE Std 1547™, *IEEE Standard for Interconnecting Distributed Resources with Electric Power Systems*, 2009

[5] A. Woyte, K. De Brabandere, D.V. Dommelen, R. Belmans, and J. Nijs, International harmonization of grid connection guidelines: adequate requirements for the prevention of unintentional islanding, *Progress in Photovoltaics: Research and Applications*, Vol. 11, p. 407-424, 2003.

[6] T. G. Habetler, R. G. Harley, Power electronic converter and system control, *Proceedings of the IEEE*, vol.89, no.6, pp.913-925, Jun 2001.

[7] Y. Sozer, D. A. Torrey, Modeling and Control of Utility Interactive Inverters, *IEEE Transactions on Power Electronics*, vol.24, no.11, pp.2475-2483, Nov. 2009

[8] L. Wu, Z. Zhao, J. Liu, A Single-Stage Three-Phase Grid-Connected Photovoltaic System With Modified MPPT Method and Reactive Power Compensation, *IEEE Transactions on Energy Conversion*, vol.22, no.4, pp.881-886, Dec. 2007

[9] Z. Chen, J. M. Guerrero, F. Blaabjerg, A Review of the State of the Art of Power Electronics for Wind Turbines, *IEEE Transactions on Power Electronics*, vol.24, no.8, pp.1859-1875, Aug. 2009

[10] J. H. Lee and B. H. Cho, Large time-scale electro-thermal simulation for loss and thermal management of power MOSFET, *in Proceedings of IEEE Power Electron Spec. Conf*., pp. 112–117, 2003.

[11] S. Yang, Q. Lei, F. Z. Peng, Z. Qian, A Robust Control Scheme for Grid-Connected Voltage-Source Inverters, *IEEE Transactions on Industrial Electronics*, vol.58, no.1, pp.202-212, Jan. 2011

[12] Xiaolin Mao, Rajapandian Ayyanar, and Harish K. Krishnamurthy, Optimal Variable Switching Frequency Scheme for Reducing Switching Loss in Single-Phase Inverters Based on Time-Domain Ripple Analysis, *IEEE Transactions on Power Electronics*, vol. 24, no. 4, April, pp. 991-1001, 2009.

[13] Bo Cao, Liuchen Chang, A Variable Switching Frequency Algorithm to Improve the Total Efficiency of Single-Phase Grid-Connected Inverters, *IEEE APEC*, pp. 2310-2315, 2013.

[14] Ilhami Colak, Ersan Kabalci, Ramazan Bayindir, Review of multilevel voltage source inverter topologies and control schemes, *International Journal on Energy Conversion and Management*, 52, pp. 1114–1128, 2011.

[15] Chen Xiaoju, Zhang Hang, Zhao Jianrong, A new Improvement Strategy based on hysteresis space vector control of Grid-connected inverter, *The International Conference on Advanced Power System Automation and Protection*, pp. 1613-1617, 2011.